Published in IET Control Theory and Applications
Received on 9th July 2009
Revised on 26th November 2009
doi: 10.1049/iet-cta.2009.0338

ISSN 1751-8644

Co-ordinated collective motion patterns in a discrete-time setting with experiments

Y. Cao D. Stuart W. Ren

Department of Electrical and Computer Engineering, Utah State University, Logan, UT 84322-4120, USA
E-mail: wren@engineering.usu.edu

Abstract: In this study, the authors co-ordinated collective motion patterns for a group of autonomous vehicles with Cartesian co-ordinate coupling in a discrete-time setting and present experimental results to validate the theoretical results. The collective motion patterns include rendezvous, circular patterns and logarithmic spiral patterns. The authors first study the collective motion patterns for a group of autonomous vehicles with single-integrator kinematics in a discrete-time setting when there exists time delay. The conditions on the network topology, the sampling period, the time delay and the Euler angle are presented such that different collective motion patterns can be achieved. The collective motion patterns for a group of autonomous vehicles with double-integrator dynamics in a discrete-time setting in the presence of relative damping are studied. The conditions on the network topology, the sampling period, the damping factor and the Euler angle are presented such that different collective patterns can be achieved. Finally, the theoretical results are experimentally validated on a multi-robot platform.

1 Introduction

The development of robot technologies has made it possible to use a group of cheap and reliable robots to finish numerous tasks in a co-operative fashion instead of using a single complicated, expensive and unreliable robot. In order to have a group of robots work cooperatively, it is important and fundamental to study the consensus problem.

Consensus means the agreement of a group of vehicles on a common state by negotiating with their local (time-varying) neighbours. Consensus has been studied extensively for single-integrator kinematics [?, 1–7], double-integrator dynamics [8–13] and rigid body attitude dynamics [14]. Traditional consensus algorithms can be simplified to a one-dimensional case by using decoupling techniques because there is no coupling among different dimensions. Detailed information about the recent study of consensus algorithms can be found in [15, 16].

Different from the traditional consensus algorithms, [17] proposed a cyclic-pursuit-based strategy in 2D in which each vehicle pursues one other vehicle along the line of sight rotated by a common offset angle. Given different offset angles, the vehicles can achieve different symmetric evenly spaced formations, namely, convergence to a single point, a circle or a logarithmic spiral pattern. Incited by [17], Ren [18, 19] introduced Cartesian co-ordinate coupling to existing consensus algorithms in 3D for, respectively, single-integrator kinematics and double-integrator dynamics under a general network topology for generating possible non-evenly spaced circular and logarithmic spiral patterns on concentric orbits with possibly non-identical radii. It was shown in [18, 19] that different collective motions, namely, converge to a single point, circular patterns with concentric orbits and logarithmic spiral curves lying in a plane perpendicular to the Euler axis, can be obtained by changing the Euler angle. The algorithms in [18, 19] are continuous-time algorithms. Noting that in reality the control inputs for physical systems are generally sampled rather than being continuous, it is useful and meaningful to study the discrete-time case of the algorithms proposed in [18, 19] and implement these algorithms on an experimental testbed.

In this paper, we study the discrete-time algorithms to achieve co-ordinated collective motions for a group of vehicles and experimentally validate the theoretical results

on a multi-robot platform. We first study the collective motion patterns for a group of vehicles with single-integrator kinematics in a discrete-time setting when there exists time delay. The conditions on the network topology, the sampling period, the time delay and the Euler angle are presented such that different motions can be achieved. Then we study the collective motion patterns for a group of vehicles with double-integrator kinematics in a discrete-time setting in the presence of relative damping. The conditions on the network topology, the sampling period, the damping factor and the Euler angle are presented such that different motions can be achieved. Both the Euler angle and the sampling period can be used to control the collective motion patterns. Finally, we provide both simulation and experimental results to validate the theoretical results. Different from the discussion in [18, 19], the sampling period also plays an important role in the discussion of this paper. In addition, the second algorithm studied in this paper considers relative damping, whereas the algorithm in [19] is based on absolute damping. As a result, the second algorithm in this paper can achieve other interesting motions. It is worth mentioning that although consensus-type algorithms have been studied extensively, few of them have been experimentally validated on an physical platform. We provide experimental results for the proposed discrete-time algorithms.

The reminder of this paper is organised as follows. In Section 2, the notations and graph theory notions are introduced as a basis. Sections 3 and 4 are the main part of this paper focusing on the study of the co-ordinated collective motion patterns for, respectively, single-integrator kinematics and double-integrator dynamics in a discrete-time setting. Simulation and experimental results are presented in Section 5. A short conclusion is given in Section 6.

2 Preliminaries and notations

2.1 Notations

The notation used in this paper is fairly standard. We use $\mathbb{R}$ and $\mathbb{C}$ to denote, respectively, the real and complex number set, $I_n \in \mathbb{R}^{n\times n}$ to denote the identity matrix, and $\mathbf{0}_{p\times q} \in \mathbb{R}^{p\times q}$ to denote an all-zero matrix. In particular, we let $\mathbf{0}_p \in \mathbb{R}^p$ and $\mathbf{1}_p \in \mathbb{R}^p$ represent, respectively, an all-zero column vector and an all-one column vector. We also use Re(·) and Im(·) to denote, respectively, the real and imaginary part of a complex number, $\bar{\cdot}$ to denote the complex conjugate of a complex number, arg(·) to denote the phase of a complex number, $\otimes$ to denote the Kronecker product of two matrices and ι to denote the imaginary unit.

2.2 Graph theory notions

For a team of n vehicles, the interaction among these vehicles can be modelled by a weighted directed graph $\mathcal{G}$ consisting of a node set $\mathcal{V} = \{1, \ldots, n\}$, an edge set $\mathcal{E} \subseteq \mathcal{V} \times \mathcal{V}$, and a weighted adjacency matrix $\mathcal{A} = [a_{ij}] \in \mathbb{R}^{n\times n}$. An edge (i, j) in a weighted directed graph denotes that vehicle j can obtain information from vehicle i, but not necessarily vice versa. The weighted adjacency matrix $\mathcal{A}$ of a weighted directed graph is defined such that a_{ij} is a positive weight if $(j, i) \in \mathcal{E}$ and $a_{ij} = 0$ otherwise.

A directed path is a sequence of edges in a directed graph of the form $(i_1, i_2), (i_2, i_3), \ldots$, where $i_j \in \mathcal{V}$. A directed graph has a directed spanning tree if there exists at least one node having a directed path to all other nodes.

Let the (non-symmetric) Laplacian matrix [20] $\mathcal{L} = [\ell_{ij}] \in \mathbb{R}^{n\times n}$ associated with $\mathcal{A}$ be defined as $\ell_{ii} = \sum_{j=1, j\neq i}^{n} a_{ij}$ and $\ell_{ij} = -a_{ij}$, $i \neq j$. From the definition of $\mathcal{L}$, it can be noted that 0 is an eigenvalue of $\mathcal{L}$ with the associated eigenvector $\mathbf{1}_n$.

3 Co-ordinated collective motion patterns for single-integrator kinematics in a discrete-time setting with time delay

Consider vehicles with discrete-time single-integrator kinematics given by

$$\frac{r_i[k+1] - r_i[k]}{T} = u_i[k] \tag{1}$$

where T is the sampling period, k is the discrete-time index, $r_i[k] = [x_i[k], y_i[k], z_i[k]]^{\mathrm{T}} \in \mathbb{R}^3$ and $u_i[k] = [u_{xi}[k], u_{yi}[k], u_{zi}[k]]^{\mathrm{T}} \in \mathbb{R}^3$ are, respectively, the state and control input for the ith vehicle at $t = kT$. When there exists sample-induced time delay, we propose the following discrete-time consensus algorithm with Cartesian co-ordinate coupling as

$$\begin{aligned} u_i[k] &= -\sum_{j=1}^{n} a_{ij} R(r_i[k-1] - r_j[k-1]),\ kT \le t < kT + h \\ u_i[k] &= -\sum_{j=1}^{n} a_{ij} R(r_i[k] - r_j[k]),\ kT + h \le t < (k+1)T \end{aligned} \tag{2}$$

for $i = 1, \ldots, n$, where a_{ij} is the (i, j)th entry of the adjacency matrix $\mathcal{A}$, h is the sample-induced time delay and $R \in \mathbb{R}^{3\times 3}$ is a rotational matrix.

We assume that h is fixed and $0 \le h < T$. Then (2) can be written in matrix form as

$$u[k] = -\frac{h}{T}(\mathcal{L} \otimes R) r[k-1] - \frac{T-h}{T}(\mathcal{L} \otimes R) r[k] \tag{3}$$

where $r[k] = [r_1[k], \ldots, r_n[k]]^{\mathrm{T}}$, $u[k] = [u_1[k], \ldots, u_n[k]]^{\mathrm{T}}$, and $\mathcal{L}$ is the (non-symmetric) Laplacian matrix associated with $\mathcal{A}$. Essentially, (3) represents the average of the control input at $kT \le t < kT + h$ and the control input

IET Control Theory Appl., 2010, Vol. 4, Iss. 11, pp. 2579–2591
doi: 10.1049/iet-cta.2009.0338

at $kT+h \le t < (k+1)T$ at sample k. Equation (3) is equivalent to (2) in terms of the average effect at each sample.

Using (3), (1) can then be written in matrix form as

$$\begin{bmatrix} r[k+1] \\ r[k] \end{bmatrix} = \underbrace{\begin{bmatrix} I_{3n}-(T-h)(\mathcal{L}\otimes R) & -h(\mathcal{L}\otimes R) \\ I_{3n} & \mathbf{0}_{3n\times 3n} \end{bmatrix}}_{\Phi} \begin{bmatrix} r[k] \\ r[k-1] \end{bmatrix} \tag{4}$$

Before moving on, we need the following definition and lemmas. In addition, some existing lemmas are stated in the appendix.

Definition 1: Let μ_i, $i=1, \ldots, n$, be the ith eigenvalue of $-\mathcal{L}$ with associated right and left eigenvectors w_i and v_i. Also let $\arg(\mu_i)=0$ for $\mu_i=0$ and $\arg(\mu_i)\in(\pi/2, 3\pi/2)$ for all $\mu_i \neq 0$. Without loss of generality, suppose that μ_i is labelled such that $\arg(\mu_1) \le \arg(\mu_2) \le \cdots \le \arg(\mu_n)$ (it follows from Lemma 7 that $\mu_1=0$, $w_1=\mathbf{1}_n$ and $v_1=\mathbf{p}$). Let λ_i, $i=1, \ldots, 3n$, be the ith eigenvalue of $-\mathcal{L}\otimes R$. Without loss of generality, let $\lambda_{3i-2}=\mu_i$, $\lambda_{3i-1}=\mu_i e^{\theta\iota}$, and $\lambda_{3i}=\mu_i e^{-\theta\iota}$.

Lemma 1: Let γ_i be the ith eigenvalue of $A\in\mathbb{R}^{n\times n}$ with associated right and left eigenvectors q_i and s_i, respectively. Also let $B=\begin{bmatrix} I_n+\beta A & \alpha A \\ I_n & \mathbf{0}_{n\times n} \end{bmatrix}$, where α and β are two positive scalars. Then the eigenvalues of B are given by $\varrho_{2i-1}=1+\beta\gamma_i+\sqrt{(1+\beta\gamma_i)^2+4\alpha\gamma_i}/2$ with associated right and left eigenvectors $\begin{bmatrix} \varrho_{2i-1}q_i \\ q_i \end{bmatrix}$ and $\begin{bmatrix} (\varrho_{2i-1}/\alpha)s_i \\ s_i \end{bmatrix}$, respectively, and $\varrho_{2i}=1+\beta\gamma_i-\sqrt{(1+\beta\gamma_i)^2+4\alpha\gamma_i}/2$, with associated right and left eigenvectors given by $\begin{bmatrix} \varrho_{2i}q_i \\ q_i \end{bmatrix}$ and $\begin{bmatrix} (\varrho_{2i}/\alpha)s_i \\ s_i \end{bmatrix}$, respectively.

Proof: Suppose that ϱ is an eigenvalue of B with a corresponding eigenvector $\begin{bmatrix} f \\ g \end{bmatrix}$, where $f, g\in\mathbb{C}^n$. Then we have $\begin{bmatrix} I_n+\beta A & \alpha A \\ I_n & \mathbf{0}_{n\times n} \end{bmatrix}\begin{bmatrix} f \\ g \end{bmatrix}=\varrho\begin{bmatrix} f \\ g \end{bmatrix}$, which implies that $f+\beta Af+\alpha Ag=\varrho f$ and $f=\varrho g$. It thus follows that $Ag=((\varrho^2-\varrho)/(\alpha+\beta\varrho))g$. Noting that $Aq_i=\gamma_i q_i$, we let $g=q_i$ and $(\varrho^2-\varrho)/(\alpha+\beta\varrho)=\gamma_i$. Therefore each γ_i corresponds to two eigenvalues of B, denoted as $\varrho_{2i-1,2i}=1+\beta\gamma_i\pm\sqrt{(1+\beta\gamma_i)^2+4\alpha\gamma_i}/2$. Therefore the right eigenvectors associated with ϱ_{2i-1} and ϱ_{2i} are, respectively, $\begin{bmatrix} \varrho_{2i-1}q_i \\ q_i \end{bmatrix}$ and $\begin{bmatrix} \varrho_{2i}q_i \\ q_i \end{bmatrix}$. By following a similar analysis, we can obtain that the left eigenvectors associated with ϱ_{2i-1} and ϱ_{2i} are, respectively, $\begin{bmatrix} (\varrho_{2i-1}/\alpha)s_i \\ s_i \end{bmatrix}$ and $\begin{bmatrix} (\varrho_{2i}/\alpha)s_i \\ s_i \end{bmatrix}$. □

Theorem 1: Suppose that the weighted directed graph $\mathcal{G}$ has a directed spanning tree. Let the control algorithm for (1) be given by (2). Let μ_i, w_i, v_i, λ_i and $\arg(\mu_i)$ be defined in Definition 1, $\mathbf{p}$ be defined in Lemma 7, and $\mathbf{a}=[a_1, a_2, a_3]^{\mathrm{T}}$, ς_k, and ϖ_k be defined in Lemma 8.

1. If $|\theta|<\theta_s^c$ where $\theta_s^c \triangleq 3\pi/2-\arg(\mu_n)$, $h<\min_{\lambda_i\neq 0}\{T, -\mathrm{Re}(\lambda_i)/|\lambda_i|^2\}$, and $T<\bar{T}$ with

$$\bar{T}=\min_{\lambda_i\neq 0}\bar{T}_i, \quad \text{where } \bar{T}_i = \frac{2(1-h^2|\lambda_i|^2)(-\mathrm{Re}(\lambda_i)-h|\lambda_i|^2)}{\mathrm{Im}(\lambda_i)^2+(-\mathrm{Re}(\lambda_i)-h|\lambda_i|^2)^2} \tag{5}$$

then Φ has exactly three eigenvalues equal to one and all other eigenvalues are within the unit circle. All vehicles will eventually rendezvous at the position

$$\left(\frac{1}{1+h}\mathbf{p}^{\mathrm{T}}x[0]+\frac{h}{1+h}\mathbf{p}^{\mathrm{T}}x[-1],\ \frac{1}{1+h}\mathbf{p}^{\mathrm{T}}y[0]+\frac{h}{1+h}\mathbf{p}^{\mathrm{T}}y[-1],\ \frac{1}{1+h}\mathbf{p}^{\mathrm{T}}z[0]+\frac{h}{1+h}\mathbf{p}^{\mathrm{T}}z[-1]\right) \tag{6}$$

where $x=[x_1, \ldots, x_n]^{\mathrm{T}}$, $y=[y_1, \ldots, y_n]^{\mathrm{T}}$, $z=[z_1, \ldots, z_n]^{\mathrm{T}}$, and $x[0]$, $x[-1]$, $y[0]$, $y[-1]$, $z[0]$ and $z[-1]$ are the initial states.

2. If $|\theta|<\theta_s^c$, $h<\min_{\lambda_i\neq 0}\{T, -\mathrm{Re}(\lambda_i)/|\lambda_i|^2\}$, $T=\bar{T}$, and there exists a unique λ_j corresponding to μ_k such that $\bar{T}_j=\bar{T}$, then Φ has exactly three eigenvalues equal to one, two eigenvalues on the unit circle, and all other eigenvalues are within the unit circle. All vehicles will eventually move on circular orbits with the centre given by (6) and the period $\pi/|\psi|$, where $\psi=|\arctan(-\mathrm{Im}(\lambda_j)/h|\lambda_j|-\mathrm{Re}(\lambda_j))|$. The radius of the orbit for vehicle i is given by $2|w_{k(i)}(v_k^{\mathrm{T}}/v_k^{\mathrm{T}}w_k\otimes\varpi_2^{\mathrm{T}}/\varpi_2^{\mathrm{T}}\varsigma_2)r(0)|\sqrt{a_2^2+a_3^2}\sin^2(\theta/2)$, where $w_{k(i)}$ is the ith component of w_k. The relative radius of the orbits is equal to the relative magnitude of $w_{k(i)}$. The relative phase of the vehicles on their orbits is equal to the relative phase of $w_{k(i)}$. The circular orbits are on a plane perpendicular to the Euler axis $\mathbf{a}$.

3. If $|\theta|<\theta_s^c$, $h<\min_{\lambda_i\neq 0}\{T, -\mathrm{Re}(\lambda_i)/|\lambda_i|^2\}$, $T>\bar{T}$, and there exists a unique λ_j associated with μ_k such that $\bar{T}_j<T$ and $\bar{T}_i>T$ for any $i\neq j$, then Φ has exactly three eigenvalues equal to one, two eigenvalues, denoted as $m_1e^{\pm m_2\iota}$ (here m_1 and m_2 are positive constants), outside the unit circle, and all other eigenvalues are within the unit circle. All vehicles will eventually move along logarithmic spiral curves with the centre given by (6), the growing rate $m_1\cos(m_2+|\theta|)$, and the period $2\pi/m_2$. The radius of the logarithmic spiral curve for vehicle i is given by $2|w_{k(i)}(v_k^{\mathrm{T}}/v_k^{\mathrm{T}}w_k\otimes\varpi_2^{\mathrm{T}}/\varpi_2^{\mathrm{T}}\varsigma_2)r(0)|e^{[m_1\cos(m_2+|\theta|)]t}\sqrt{a_2^2+a_3^2}\sin^2(\theta/2)$. The relative radius of the logarithmic spiral curves is equal to the relative magnitude of $w_{k(i)}$. The relative phase of the

vehicles on their curves is equal to the relative phase of $w_{k(i)}$. The logarithmic spiral curves are on a plane perpendicular to the Euler axis **a**.

Proof: From Lemma 1, the eigenvalues of Φ are given by $\varrho = 1 - (T - h)\lambda_i \pm \sqrt{(1 - (T - h)\lambda_i)^2 - 4h\lambda_i}/2$. It follows that the eigenvalues of Φ satisfy

$$s[s - 1 - (T - h)\lambda_i] - h\lambda_i = 0 \tag{7}$$

When $\lambda_i = 0$, it follows that the two roots of (7) are 1 and 0. When $\lambda_i \neq 0$, applying bilinear transformation to (7) gives

$$-T\lambda_i t^2 + 2(1 + h\lambda_i)t + 2 + (T - 2h)\lambda_i = 0 \tag{8}$$

From Lemma 5, the roots of (7) are within the unit circle if and only if the roots of (8) are in the open left half-plane. Let the two roots of (8) be t_1 and t_2. It follows from (8) that

$$t_1 + t_2 = \frac{2(1 + h\lambda_i)}{T\lambda_i} = 2\frac{(\bar{\lambda}_i/|\lambda_i|^2) + h}{T} \tag{9}$$

To guarantee that both t_1 and t_2 are in the open left half plane, the right side of (9) should have a negative real part, that is, $h < -\mathrm{Re}(\lambda_i)/|\lambda_i|^2$. Meanwhile, the bound of T is the critical value of T under which one root of (9) is on the imaginary axis. Without loss of generality, assume $t_1 = \chi\iota$, where χ is a real number. Substituting $t_1 = \chi\iota$ into (9) gives

$$\chi^2 T[\mathrm{Re}(\lambda_i) + \mathrm{Im}(\lambda_i)\iota] + 2[1 + h(\mathrm{Re}(\lambda_i) + \mathrm{Im}(\lambda_i)\iota)]\chi\iota + 2 + (T - 2h)[\mathrm{Re}(\lambda_i) + \mathrm{Im}(\lambda_i)\iota] = 0$$

which can be written as two equations by separating, respectively, the real and imaginary parts. After some manipulations, we can obtain that $T = \bar{T}_i$, where $\bar{T}_i$ defined in (5). To guarantee that $\bar{T}_i > 0$, we need the following two inequalities

$$1 - h^2|\lambda_i|^2 > 0, \qquad -\mathrm{Re}(\lambda_i) - h|\lambda_i|^2 > 0$$

After some simplifications, we have that $\bar{T}_i > 0$ if $h < -\mathrm{Re}(\lambda_i)/|\lambda_i|^2$.

1. When $|\theta| < \theta_s^c$, it follows from the proof of Theorem 1 in [18] that all eigenvalues of $-\mathcal{L} \otimes R$, that is, all λ_i, will have negative real parts except for three zero eigenvalues. When $h < \min_{\lambda_i \neq 0}\{T, -\mathrm{Re}(\lambda_i)/|\lambda_i|^2\}$, and $T < \bar{T}$, it follows from the discussion in the previous paragraph that all eigenvalues of Φ are within the unit circle except for three eigenvalues equal to one. Note from Lemma 1 that the right and left eigenvectors corresponding to $\lambda_{2\ell-1}$ are $\begin{bmatrix} \mathbf{1}_n \otimes \mathfrak{s}_\ell \\ \mathbf{1}_n \otimes \mathfrak{s}_\ell \end{bmatrix}$ and $h/h + 1\begin{bmatrix} \frac{1}{h}\mathbf{p} \otimes \boldsymbol{\varpi}_\ell \\ \mathbf{p} \otimes \boldsymbol{\varpi}_\ell \end{bmatrix}$, where $\ell = 1, 2, 3$. By following the proof of Case 2 of Theorem 1 in [19], we can obtain that $x_i[k] \to (1/(1 + h))\mathbf{p}^{\mathrm{T}}x[0] + (h/(1 + h))\mathbf{p}^{\mathrm{T}}x[-1]$, $y_i[k] \to (1/(1 + h))\mathbf{p}^{\mathrm{T}}y[0] + (h/(1 + h))\mathbf{p}^{\mathrm{T}}y[-1]$, $z_i[k] \to (1/(1 + h))\mathbf{p}^{\mathrm{T}}z[0] + (h/(1 + h))\mathbf{p}^{\mathrm{T}}z[-1]$ for large k.

2. Similar to the proof of 1, when $|\theta| < \theta_s^c$, all eigenvalues of $-\mathcal{L} \otimes R$ will have negative real parts except for three zero eigenvalues. When $h < \min_{\lambda_i \neq 0} -2\mathrm{Re}(\lambda_i)/3|\lambda_i|^2$, $T = \bar{T}$, and there exists a unique λ_j corresponding μ_k such that $\bar{T}_i = \bar{T}$, all eigenvalues of Φ are within the unit circle except for three eigenvalues equal to one and two other eigenvalues on the unit circle. In addition, it can be computed that the two eigenvalues are $(-\mathrm{Im}(\lambda_j)\iota + h|\lambda_j|^2 - \mathrm{Re}(\lambda_j))/(-\mathrm{Im}(\lambda_j)\iota - h|\lambda_j|^2 + \mathrm{Re}(\lambda_j))$ and $(-\mathrm{Im}(\lambda_j)\iota - h|\lambda_j|^2 + \mathrm{Re}(\lambda_j))/(-\mathrm{Im}(\lambda_j)\iota + h|\lambda_j|^2 - \mathrm{Re}(\lambda_j))$. By writing these two eigenvalues as $e^{\pm 2\psi\iota}$, where $\psi = \arctan(-\mathrm{Im}(\lambda_j)/h|\lambda_j| - \mathrm{Re}(\lambda_j))$, it follows from the proof of Theorem 1 in [18] that all vehicles will move in circular orbits with the centre given by (6) and the period $\pi/|\psi|$. Similarly, we can also compute the radius of the orbit, the relative phase and the relationship between the circular orbits and the Euler axis **a** by following a similar analysis to the proof of Theorem 1 in [18].

3. The proof is similar to that of Case 3 of Theorem 1 in [18] and is therefore omitted here. □

Remark 1: In Theorem 1, given a constant sampling period T satisfying $T < \bar{T}$, where $\bar{T}$ is defined in Theorem 1, we can also analyse the critical value of θ by following a similar analysis. When the Euler angle θ is below, equal to, or above the critical value, different collective motions can also be achieved. Different from the continuous-time case in [18] where the critical value of θ was given explicitly and analytically, the critical value of θ in the discrete-time case is, in general, hard to be derived analytically. However, given T, h and $\mathcal{L}$, the critical value of θ can be obtained numerically.

Remark 2: Note that the continuous-time controller in [18] represents the ideal case of (2) when $T \to 0$ and $h \to 0$. Accordingly, the continuous-time algorithm in [18] works better than the discrete-time algorithm (2). However, the discrete-time algorithm (2) represents a more realistic scenario and therefore can be directly applied in real systems.

4 Co-ordinated collective motion patterns for double-integrator dynamics in a discrete-time setting with relative damping

For vehicles with discrete-time double-integrator dynamics given by

$$\begin{aligned} r_i[k + 1] &= r[k] + Tv_i[k] \\ v_i[k + 1] &= v_i[k] + Tu_i[k], \quad i = 1, \ldots, n \end{aligned} \tag{10}$$

doi: 10.1049/iet-cta.2009.0338

where T is the sampling period, k is the discrete-time index, $r_i[k] = [x_i[k], y_i[k], z_i[k]]^{\mathrm{T}} \in \mathbb{R}^3$ and $v_i[k] = [v_{xi}[k], v_{yi}[k], v_{zi}[k]]^{\mathrm{T}} \in \mathbb{R}^3$ are the position and velocity, and $u_i[k] = [u_{xi}[k], u_{yi}[k], u_{zi}[k]]T \in \mathbb{R}^3$ is the control input associated with the ith vehicle at $t = kT$, we consider a consensus algorithm with Cartesian co-ordinate coupling as

$$u_i[k] = -\sum_{j=1}^{n} a_{ij} R[(r_i[k] - r_j[k]) + \gamma(v_i[k] - v_j[k])],$$
$$i = 1, \ldots, n \tag{11}$$

where a_{ij} is the (i, j)th entry of the adjacency matrix $\mathcal{A}$, γ is a positive constant and $R \in \mathbb{R}^{3\times 3}$ is a rotation matrix.

Using (11), (10) can be written in matrix form as

$$\begin{bmatrix} r[k+1] \\ v[k+1] \end{bmatrix} = (I_{6n} + T\Psi)\begin{bmatrix} r[k] \\ v[k] \end{bmatrix}$$

where $r = [r_1^{\mathrm{T}}, \ldots, r_n^{\mathrm{T}}]^{\mathrm{T}}$, $v = [v_1^{\mathrm{T}}, \ldots, v_n^{\mathrm{T}}]^{\mathrm{T}}$, $\Psi = \begin{bmatrix} \mathbf{0}_{3n\times 3n} & I_{3n} \\ -\mathcal{L}\otimes R & -\gamma\mathcal{L}\otimes R \end{bmatrix}$ and $\mathcal{L}$ is the (non-symmetric) Laplacian matrix associated with $\mathcal{A}$. We next study the eigenvalues of Ψ.

The characteristic polynomial of Ψ is given by

$$\det(sI_{6n} - \Psi) = \det\left(\begin{bmatrix} sI_{3n} & -I_{3n} \\ \mathcal{L}\otimes R & sI_{3n} + \gamma\mathcal{L}\otimes R \end{bmatrix}\right)$$
$$= \det(s^2 I_{3n} + (\gamma s + 1)\mathcal{L}\otimes R)$$

where we have used Lemma 4 to derive the last equality. Letting λ_i, $i = 1, \ldots, 3n$, be defined in Definition 1, it follows that the eigenvalues of Ψ satisfy

$$s^2 - \gamma\lambda_i s - \lambda_i = 0 \tag{12}$$

Note that each eigenvalue of $-\mathcal{L}\otimes R$, λ_i, corresponding to two eigenvalues of Ψ, denoted as μ_{2i-1} and μ_{2i}. Before moving on, we need the following lemmas.

Lemma 2 [21]: Suppose that $\mathrm{Im}(\lambda_i) \neq 0$ and $\mathrm{Re}(\lambda_i) < 0$. Then $\mathrm{Re}(\mu_{2i-1}) < 0$ and $\mathrm{Re}(\mu_{2i}) < 0$ if and only if $\gamma > \bar{\gamma}_i$, where $\bar{\gamma}_i \triangleq \sqrt{\mathrm{Im}(\lambda_i)^2/-\mathrm{Re}(\lambda_i)|\lambda_i|^2}$.

Lemma 3: Let γ_i be the ith eigenvalue of $A \in \mathbb{R}^{n\times n}$ with associated right and left eigenvectors q_i and s_i, respectively. Also let $B = \begin{bmatrix} \mathbf{0}_{n\times n} & I_n \\ -A & -\alpha A \end{bmatrix}$, where α is a positive scalar. Then the eigenvalues of B are given by $\varrho_{2i-1} = -\alpha\gamma_i + \sqrt{\gamma_i^2\alpha^2 + 4\gamma_i}/2$ with associated right and left eigenvectors $\begin{bmatrix} q_i \\ \varrho_{2i-1}q_i \end{bmatrix}$ and $\begin{bmatrix} 1 + \alpha\varrho_{2i-1}/\varrho_{2i-1}s_i \\ s_i \end{bmatrix}$, respectively, and $\varrho_{2i} = \alpha\gamma_i - \sqrt{\gamma_i^2\alpha^2 + 4\gamma_i}/2$, with associated right and left eigenvectors given by $\begin{bmatrix} q_i \\ \varrho_{2i}q_i \end{bmatrix}$ and $\begin{bmatrix} 1 + (\alpha\varrho_{2i}/\varrho_{2i})s_i \\ s_i \end{bmatrix}$, respectively.

Proof: The proof follows a similar analysis to that of Lemma 1. □

Theorem 2: Suppose that the weighted directed graph $\mathcal{G}$ has a directed spanning tree. Define $\bar{\gamma} \triangleq \max_i \bar{\gamma}_i$, where $\bar{\gamma}_i$ is defined in Lemma 2. Let the control algorithm for (10) be given by (11). Let μ_i, w_i, ν_i, λ_i and $\arg(\mu_i)$ be defined in Definition 1, $\mathbf{p}$ be defined in Lemma 7, and $\mathbf{a} = [a_1, a_2, a_3]^{\mathrm{T}}$, ς_k, and ϖ_k be defined in Lemma 8. Denote $\bar{\tau} = \min_{\lambda_i \neq 0} 2\mathrm{Re}(\lambda_i)/|\lambda_i|^2$.

1. Suppose that $R = I_3$. All vehicles will eventually rendezvous at the position

$$(\mathbf{p}x[0] + kT\mathbf{p}v_x[0], \mathbf{p}y[0] + kT\mathbf{p}v_y[0], \mathbf{p}z[0] + kT\mathbf{p}v_z[0]) \tag{13}$$

for large k if and only if $\gamma > \bar{\gamma}$ and $T < \bar{\tau}$, where x, y, z, v_x, v_y and v_z are, respectively, stack vectors of x_i, y_i, z_i, v_{xi}, v_{yi} and v_{zi}, and $x[0]$, $y[0]$, $z[0]$, $v_x[0]$, $v_y[0]$ and $v_z[0]$ are the initial states (Note that the rendezvous position might be time varying in contrast to a constant rendezvous position in [19].).

2. Suppose that $\gamma > \bar{\gamma}$ and $T < \bar{\tau}$. Given $|\mu_i|$, $i = 2, \ldots, n$, let θ_d^{ℓ} be the maximal Euler angle such that the roots of (12) are on the imaginary axis for some i and the roots of (12) are in the left half-plane for any other i. If $|\theta| < \theta_d^{\ell}$, then all vehicles will eventually rendezvous at the position (13).

3. Assume that $|\theta| < \theta_d^{\ell}$, $\gamma > \bar{\gamma}$, $T = \bar{\tau}$, and there exists a unique λ_j associated with μ_k such that $2\mathrm{Re}(\lambda_j)/|\lambda_j|^2 = \bar{\tau}$. Then $I_{6n} + TM$ has exactly six eigenvalues equal to one and two eigenvalues on the unit circle and all other eigenvalues are within the unit circle. All vehicles will eventually move on circular orbits with the centre given by (13) and the period $2\pi/\psi$, where $\psi = |\arctan(1 + T\mathrm{Re}(\sigma_{6\kappa-3})/T\mathrm{Im}(\sigma_{6\kappa-3}))|$ with $\sigma_{6\kappa-3} = -\gamma\lambda_j + \sqrt{\lambda_j^2\gamma^2 + 4\lambda_j}/2$. The radius of the orbit for vehicle i is given by $2|w_{\kappa(i)}p_c^{\mathrm{T}}[r(0)^{\mathrm{T}}, v(0)^{\mathrm{T}}]^{\mathrm{T}}|\sqrt{a_2^2 + a_3^2}\sin^2(\theta/2)$, where $w_{\kappa(i)}$ is the ith component of w_κ and $p_c = 1/(1 + \gamma\sigma_{6\kappa-3}/\sigma_{6\kappa-3} + \sigma_{6\kappa-3})\nu_\kappa^{\mathrm{T}} w_\kappa \varpi_2^{\mathrm{T}} \varsigma_2 \begin{bmatrix} 1 + \gamma\sigma_c/\sigma_c(\nu_\kappa \otimes \varpi_2) \\ \nu_\kappa \otimes \varpi_2 \end{bmatrix}$, where $\sigma_c = \iota\psi$. The relative radius of the orbits is equal to the relative magnitude of $w_{\kappa(i)}$. The relative phase of the vehicles on their orbits is equal to the relative phase of $w_{\kappa(i)}$. The circular orbits are on a plane perpendicular to the Euler axis $\mathbf{a}$.

4. Assume that $|\theta| < \theta_d^{\ell}$, $\gamma > \bar{\gamma}$, $T > \bar{\tau}$, and there exists a unique λ_j associated with μ_k such that $2\mathrm{Re}(\lambda_j)/|\lambda_j|^2 < T$ and $2\mathrm{Re}(\lambda_i)/|\lambda_i|^2 > T$ for any $i \neq j$. Then $I_{6n} + TM$ has exactly six eigenvalues equal to one, two eigenvalues,

denoted as $m_1 e^{\pm m_2 \iota}$ (Here m_1 and m_2 are positive constants.), outside the unit circle, and all other eigenvalues are within the unit circle. All vehicles will eventually move along logarithmic spiral curves with centre given by (13), growing rate m_1, and period $2\pi/m_2$. The radius of the logarithmic spiral curve for vehicle i is $2|w_{\kappa(i)} p_c^{\mathrm{T}}[r(0)^{\mathrm{T}}, \ v(0)^{\mathrm{T}}]^{\mathrm{T}} e^{m_1 t}\sqrt{a_2^2 + a_3^2}\sin^2(\theta/2)$, where p_c is defined in Case 3. The relative radius of the logarithmic spiral curves is equal to the relative magnitude of $w_{\kappa(i)}$. The relative phase of the vehicles on their curves is equal to the relative phase of $w_{\kappa(i)}$. The curves are on a plane perpendicular to the Euler axis **a**.

Proof:

1. When $R = I_3$, it follows from Lemma 6 that μ_i is an eigenvalue of $-\mathcal{L} \otimes R$ with algebraic multiplicity 3. When $\mathcal{G}$ has a directed spanning tree, it follows from Lemma 7 that all the eigenvalues of $-\mathcal{L}$ are in the open left half-plane except for one zero eigenvalue. Therefore $-\mathcal{L} \otimes R$ has exactly three zero eigenvalues and other eigenvalues are in the open left half-plane if $\mathcal{G}$ has a directed spanning tree. When $\lambda_i = 0$, two roots of (12) are equal to zero. When $\lambda_i \neq 0$ and $\mathrm{Im}(\lambda_i) = 0$, it follows from (12) that the two roots are in the open left half-plane. When $\mathrm{Im}(\lambda_i) \neq 0$, it follows from Lemma 2 that the two roots are in the open left half-plane if $\gamma > \bar{\gamma}_i$. Therefore if $\gamma > \bar{\gamma}$, Ψ has six zero eigenvalues and all other eigenvalues are in the open left half-plane, which then implies that $I_{6n} + T\Psi$ has exactly six eigenvalues equal to one and all other eigenvalues are within the unit circle when $T < \bar{\tau}$ and $\gamma > \bar{\gamma}$. Note also that the left and right eigenvectors corresponding to $\mu_{2i-1,2i}$ can be derived by following Lemma 3. The proof follows a similar analysis to that in the proof of Theorem 1 in [19].

2. When $|\theta| < \theta_d^c$ $\gamma > \bar{\gamma}$ and $T < \bar{\tau}$, by following a similar analysis to that in the proof of case 1), we have that the eigenvalues of $I_{6n} + \Psi$ are within the unit circle except for six eigenvalues equal to one. The final states of the vehicles can also be analysed by following case 1).

3. For the third statement, if $\theta < \theta_d^c$, $\gamma > \bar{\gamma}$, $T = \bar{\tau}$, and there exists a unique λ_j associated with μ_k such that $2\mathrm{Re}(\lambda_j)/|\lambda_j|^2 = \bar{\tau}$, $I_{6n} + T\Psi$ has exactly six eigenvalues equal to one, two eigenvalues on the unit circle, and all other eigenvalues are within the unit circle. Meanwhile, we can obtain that the two eigenvalues of Ψ associated with λ_j are given by $\sigma_{6\kappa-3} = -\gamma\lambda_j + \sqrt{\lambda_j^2\gamma^2 + 4\lambda_j}/2$ and $\overline{\sigma_{6\kappa-3}}$, which implies that the two eigenvalues of $I_{6n} + T\Psi$ associated with $\sigma_{6\kappa-3}$ and $\overline{\sigma_{6\kappa-3}}$ are given by $1 + T\mathrm{Re}(\sigma_{6\kappa-3}) + T\mathrm{Im}(\sigma_{6\kappa-3})\iota$ and $1 + T\mathrm{Re}(\sigma_{6\kappa-3}) - T\mathrm{Im}(\sigma_{6\kappa-3})\iota$. Note from Lemma 3 that the right and left eigenvectors associated with $\sigma_{6\kappa-3}$ are, respectively, $\begin{bmatrix} w_\kappa \otimes \varsigma_2 \\ \sigma_{6\kappa-3}(w_\kappa \otimes \varsigma_2) \end{bmatrix}$ and $\begin{bmatrix} 1 + \gamma\sigma_{6\kappa-3}/\sigma_{6\kappa-3}(\nu_\kappa \otimes \varpi_2) \\ \nu_\kappa \otimes \varpi_2 \end{bmatrix}$. We can choose $m_{6\kappa-3} = \begin{bmatrix} w_\kappa \otimes \varsigma_2 \\ \sigma_{6\kappa-3}(w_\kappa \otimes \varsigma_2) \end{bmatrix}$ and $p_{6\kappa-3} = 1/(1 + \gamma\sigma_{6\kappa-3}/\sigma_{6\kappa-3} + \sigma_{6\kappa-3})$ $\nu_\kappa^{\mathrm{T}} w_\kappa \varpi_2^{\mathrm{T}} \varsigma_2 \begin{bmatrix} 1 + \gamma\sigma_{6\kappa-3}/\sigma_{6\kappa-3}(\nu_\kappa \otimes \varpi_2) \\ \nu_\kappa \otimes \varpi_2 \end{bmatrix}$. Note that $p_{6\kappa-3}^T m_{6\kappa-3} = 1$. Similarly, it follows that the right and left eigenvectors corresponding to $\overline{\sigma_{6\kappa-3}}$ are given by $\overline{m_{6\kappa-3}}$ and $\overline{p_{6\kappa-3}}$. The following proof then follows from that in Theorem 1 in [19].

4. The proof is similar to that of Case 4) of Theorem 1 in [19] and is therefore omitted here. □

Remark 3: In Theorem 2, given a constant coupling gain γ satisfying $\gamma < \bar{\gamma}$, where $\bar{\gamma}$ is defined in Lemma 2, we can also analyse the critical value of θ by following a similar analysis. When the Euler angle θ is below, equal to, or above the critical value, different collective motions can also be achieved. Note again that given T, γ, and $\mathcal{L}$, the critical value of θ can be obtained numerically.

Remark 4: From Theorem 2, the algorithm (11) achieves different motions from the algorithm in [19]. In particular, the centre of all vehicles using (11) might keep moving ultimately whereas the centre of all vehicles using the algorithm in [19] remains static ultimately.

5 Simulation and experimental validation

In this section, we provide simulation and experimental results to validate the theoretical results in Sections 3 and 4. For simulations and experiments for both single-integrator kinematics and double-integrator dynamics, the (non-symmetric) interaction graph is chosen as in Fig. 1 with the corresponding (non-symmetric) Laplacian matrix chosen as

$$\begin{bmatrix} 1.5 & 0 & -1 & -0.5 \\ -1.2 & 1.2 & 0 & 0 \\ -0.1 & -0.9 & 1 & 0 \\ -1 & 0 & 0 & 1 \end{bmatrix}$$

It can be noted that the interaction graph has a directed spanning tree.

5.1 Matlab/simulink simulation results

For the algorithm (2), three different values of θ are chosen. In all plots hereafter, circles represent the starting positions of the robots and squares denote the ending positions of the robots.

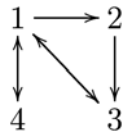

Figure 1 *Directed graph $\mathcal{G}$ for four vehicles*

Arrow from j to i denotes that vehicle i can receive information from vehicle j

doi: 10.1049/iet-cta.2009.0338

We let $T = 0.1$ s and $h = 0.02$ s. When $\theta = 0.7$ rad, the trajectories are shown in Fig. 2*a*. It can be noted that the four vehicles ultimately rendezvous. When $\theta = 1.2133$ rad, the trajectories are shown in Fig. 2*c* where the four vehicles ultimately move on separate circular orbits. When $\theta = 1.35$ rad, the trajectories are shown in Fig. 2*e* where the four vehicles move along logarithmic spiral curves. These simulation results validate the theoretical results in Theorem 1.

Similar to the single-integrator kinematics case, three different values of θ are chosen for the double-integrator dynamics case. We let $T = 0.1$ s. When $\theta = 0.7$ rad, the trajectories of the four vehicles are shown in Fig. 2*b*. It can be noted that the four vehicles ultimately rendezvous while they keep moving because of the relative damping. When $\theta = 1.1$ rad, the trajectories of the four vehicles are shown in Fig. 3*d*. It can be noted that the four vehicles ultimately move on separate circular orbits while the center of the circular orbits keeps moving. When $\theta = 1.3$ rad, the trajectories of the four vehicles are shown in Fig. 3*f*. It can be noted that the four vehicles ultimately spiral along logarithmic curves while the centre of the spiral curves keeps moving. The simulation results validate the theoretical results in Theorem 2.

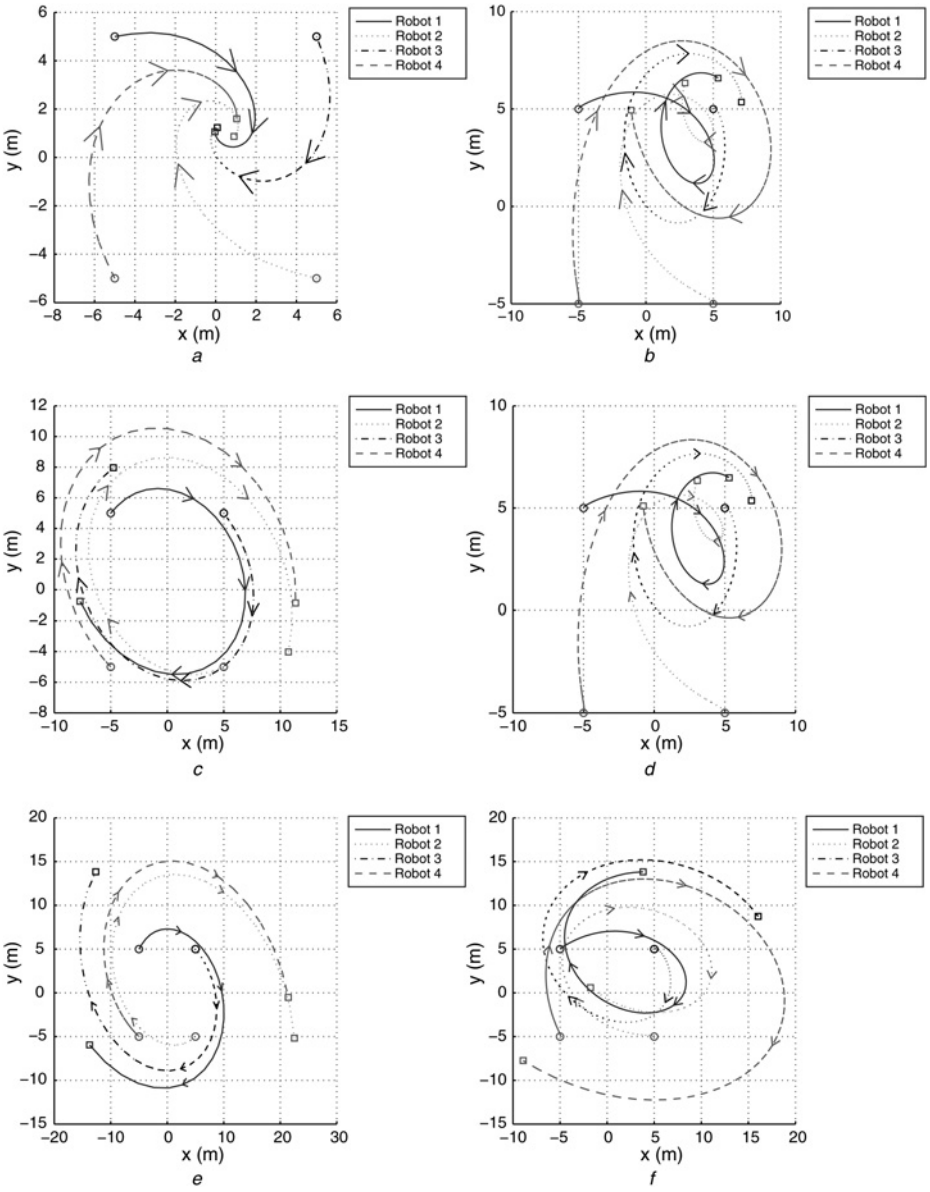

Figure 2 *Simulation results using (2) and (11)*

a Simulation results using (2) when $\theta = 0.7$ rad, $T = 0.1$ s and $h = 0.02$ s
b Simulation results using (11) when $\theta = 1$ rad and $T = 0.1$ s
c Simulation results using (2) when $\theta = 1.2133$ rad, $T = 0.1$ s, and $h = 0.02$ s
d Simulation results using (11) when $\theta = 1.1$ rad and $T = 0.1$ s
e Simulation results using (2) when $\theta = 1.35$ rad, $T = 0.1$ s, and $h = 0.02$ s
f Simulation results using (11) when $\theta = 1.3$ rad and $T = 0.1$ s

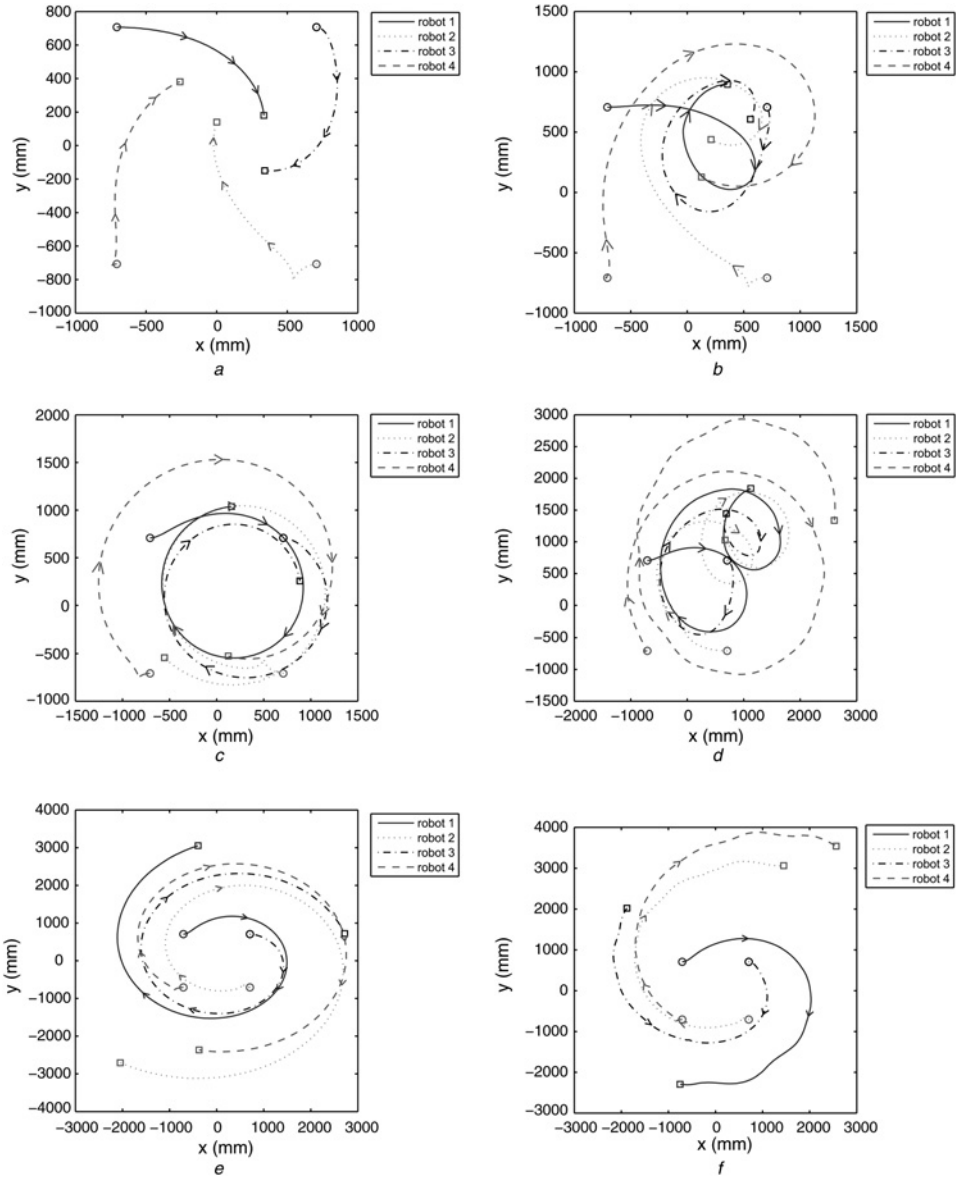

Figure 3 *Experimental results using (2) and (11)*

a Experimental results using (2) when $\theta = 0.7$ rad
b Experimental results using (11) when $\theta = 1$ rad
c Experimental results using (2) when $\theta = 1.2133$ rad
d Experimental results using (11) when $\theta = 1.1$ rad
e Experimental results using (2) when $\theta = 1.35$ rad
f Experimental results using (11) when $\theta = 1.3$ rad

5.2 Experimental validation

In this section, we provide experimental results to validate the theoretical results in Sections 3 and 4 on a multi-robot platform.

5.2.1 Robot platform and program implementation: The physical robot experiments are based on four AmigoBots as shown in Fig. 4 from ActivMedia Robotics. All four robots are driven via differential drive. They have high-precision wheel encoders and eight sonar attached around the robot. An AmigoBot

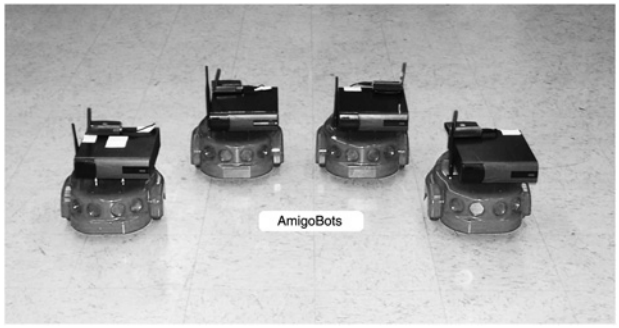

Figure 4 *Four AmigoBots*

doi: 10.1049/iet-cta.2009.0338

uses encoders/decoders to calculate the distance travelled as well as its rotational angle (i.e. the orientation of the robot). Within each robot is a 16-bit micro-controller that maintains support for all sensor and actuation features of the robot. For an AmigoBot, a host computer acts as the high-level control whereas the low-level control is performed on board the robot with the micro-controller. A control program is then run remotely over a WAN. The host computer executes programs which send and receive sensor data and control actuation to the robots on board the micro-controller. The relative communication delay between the host computer and each robot is 100 ms (i.e. the sampling period T is 100 ms).

The control program platform allows for emulating interaction between robots including the interaction topology. The testbed program platform is set up with two tiers. The top tier is responsible for executing the control algorithms and sending and receiving the control commands and sensor data to and from the robot's micro-

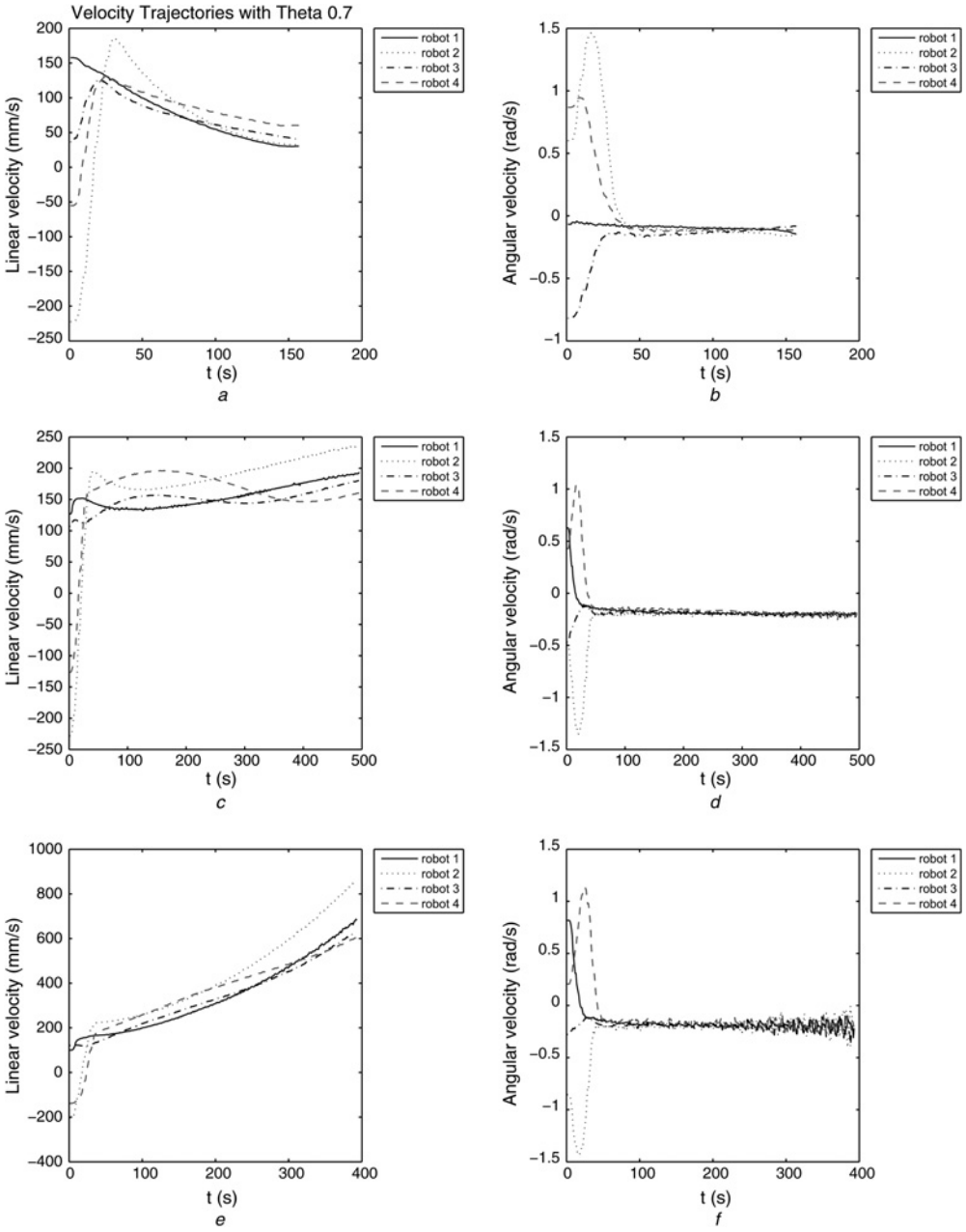

Figure 5 *Linear and angular velocities using (2)*

a Linear velocities when $\theta = 0.7$ rad
b Angular velocities when $\theta = 0.7$ rad
c Linear velocities when $\theta = 1.2133$ rad
d Angular velocities when $\theta = 1.2133$ rad
e Linear velocities when $\theta = 1.35$ rad
f Angular velocities when $\theta = 1.35$ rad

controller. In this tier, the communication topology can be set up by enabling or disabling the communication between any pair of robots. The bottom tier is responsible for sensor data acquisition and direct PID loop control. In this tier, the micro-controller will collect the state information from the sensors and tell the physical robot how to actuate based on the received control commands. More detailed information can be found in [22].

5.2.2 Robot modelling: The differential drive system of the ground robot can be described by the kinematic equations as

$$\begin{aligned} \dot{x}_i &= v_i \cos(\theta_i) \\ \dot{y}_i &= v_i \sin(\theta_i) \\ \dot{\theta}_i &= \omega_i \end{aligned} \tag{14}$$

where x_i and y_i are the positions of the centre of the robot, θ_i is the orientation of rotation of the robot and v_i and ω_i are the linear and angular velocities of the robot. The robot has a non-holonomic constraint $\dot{x}_i \sin(\theta_i) - \dot{y}_i \cos(\theta_i) = 0$.

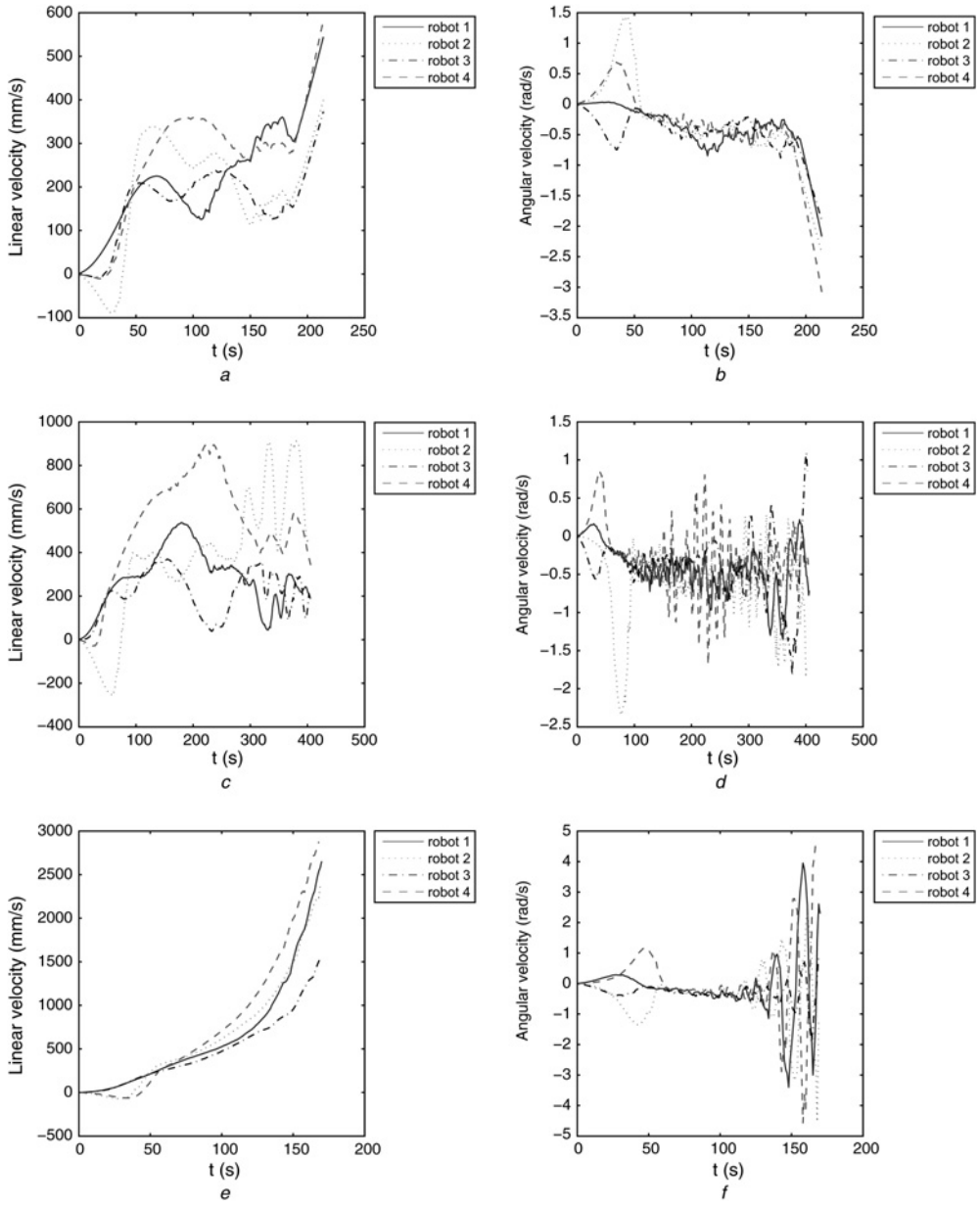

Figure 6 *Linear and angular velocities using (11)*

a Linear velocities when $\theta = 1$ rad
b Angular velocities when $\theta = 1$ rad
c Linear velocities when $\theta = 1.1$ rad
d Angular velocities when $\theta = 1.1$ rad
e Linear velocities when $\theta = 1.3$ rad
f Angular velocities when $\theta = 1.3$ rad

doi: 10.1049/iet-cta.2009.0338

To avoid using the non-linear model of kinematics, we feedback linearise (14) for a fixed point off the centre of the wheel axis denoted as (x_{bi}, y_{bi}), where $x_{bi} = x_i + L_i\cos(\theta_i)$ and $y_{bi} = y_i + L_i\sin(\theta_i)$ with L_i representing the distance between this fixed point and the centre of the wheel axis. Therefore the whole system can be described as

$$\begin{bmatrix} \dot{x}_{bi} \\ \dot{y}_{bi} \end{bmatrix} = \begin{bmatrix} \cos(\theta_i) & -L_i\sin(\theta_i) \\ \sin(\theta_i) & L_i\cos(\theta_i) \end{bmatrix} \begin{bmatrix} v_i \\ \omega_i \end{bmatrix}$$

Letting

$$\begin{bmatrix} v_i \\ \omega_i \end{bmatrix} = \begin{bmatrix} \cos(\theta_i) & -L_i\sin(\theta_i) \\ \sin(\theta_i) & L_i\cos(\theta_i) \end{bmatrix}^{-1} \begin{bmatrix} u_{xi} \\ u_{yi} \end{bmatrix} \quad (15)$$

we obtain

$$\begin{aligned} \dot{x}_{bi} &= u_{xi} \\ \dot{y}_{bi} &= u_{yi} \end{aligned} \quad (16)$$

where u_{xi} and u_{yi} are the control variables to be designed. It can be noted that (16) takes in the form of a single-integrator kinematics with respect to the point (x_{bi}, y_{bi}). Once u_{xi} and u_{yi} are designed, the linear velocity v_i and angular velocity ω_i can be calculated according to (15). The linear velocity v_i and angular velocity ω_i are the control commands to the physical robot. Similarly, by letting $\dot{u}_{xi} = \tau_{xi}$ and $\dot{u}_{yi} = \tau_{yi}$, a double-integrator dynamics model can be obtained by designing the control inputs τ_{xi} and τ_{yi}. To validate the aforementioned algorithms in Sections 3 and 4, we have chosen $L_i = 0.15$ m in this paper.

5.2.3 Experimentation results: The above two controllers for the simulation were implemented in C++ code on the testbed program. The same topology was used as before, but with a gain to make the values smaller. The physical robots are very sensitive to gains in actuation therefore a gain of '0.001' was implemented to prevent control inputs from saturating the motors. The robots are also driven with both a velocity and angular velocity command. Therefore on the controller for double-integrator dynamics, the values obtained for control inputs of acceleration are integrated before being sent to the robot.

1. *Collective motion patterns for single-integrator kinematics:* In this case, three different values of θ are chosen. When θ is set to 0.7 rad, the four robots spiral inward to rendezvous as in Fig. 3*a*. Note that these data represent the actual encoder information from the robot. Therefore when the four robots converge, the data points do not meet because they represent the centre of each physically spaced robot. When θ is set to 1.2133 rad, the four robots ultimately move on separate circular orbits, as in Fig. 3*c*. When θ is set to 1.35 rad, the four robots spiral out as seen in Fig. 3*e*. In addition, the linear and angular velocities of the robots are shown in Fig. 5.

2. *Collective motion patterns for double-integrator dynamics:* In this case, three different values of θ are also chosen. When θ is set to 1.0 rad, the four robots spiral inward to rendezvous as shown in Fig. 3*b*. Note that the four robots will converge and then keep moving because of the relative damping. When θ is set to 1.1 rad, the four robots which follow ultimately move on separate circular orbits as the centre of the circular orbits keep moving as shown in Fig. 3*d*. When θ is set to 1.3 rad, the four robots spiral out as the centre of the spiral curves keep moving as shown in Fig. 3*f*. In addition, the linear and angular velocities of the robots are shown in Fig. 6.

6 Conclusion

This paper focused on the study of the co-ordinated collective motion patterns for a group of autonomous vehicles with Cartesian co-ordinate coupling in a discrete-time setting. We first studied conditions on the network topology, the sampling period, the time delay and the Euler angle such that different collective motion patterns can be achieved for single-integrator kinematics in the presence of time delay. Then we studied the conditions on the network topology, the damping factor and the Euler angle such that different collective motions patterns for double-integrator dynamics in the presence of relative damping. Experimental results on a multi-robot platform were employed to show the effectiveness of the theoretical results.

7 References

[1] JADBABAIE A., LIN J., MORSE A.S.: 'Coordination of groups of mobile autonomous agents using nearest neighbor rules', *IEEE Trans. Autom. Control*, 2003, **48**, (6), pp. 988–1001

[2] OLFATI-SABER R., MURRAY R.M.: 'Consensus problems in networks of agents with switching topology and time-delays', *IEEE Trans. Autom. Control*, 2004, **49**, (9), pp. 1520–1533

[3] MOREAU L.: 'Stability of multi-agent systems with time-dependent communication links', *IEEE Trans. Autom. Control*, **50**, (2), pp. 169–182

[4] REN W., BEARD R.W.: 'Consensus seeking in multiagent systems under dynamically changing interaction topologies', *IEEE Trans. Autom. Control*, 2005, **50**, (5), pp. 655–661

[5] XIAO F., WANG L.: 'Asynchronous consensus in continuous-time multi-agent systems with switching topology and time-varying delays', *IEEE Trans. Autom. Control*, 2008, **53**, (8), pp. 1804–1816

[6] CAO M., MORSE A.S., ANDERSON B.D.O.: 'Agreeing asynchronously', *IEEE Trans. Autom. Control*, 2008, **53**, (8), pp. 1826–1838

[7] FANG L., ANTSAKLIS P.J.: 'Asynchronous consensus protocols using nonlinear paracontractions theory', *IEEE Trans. Autom. Control*, 2008, **53**, (10), pp. 2351–2355

[8] FAX J.A., MURRAY R.M.: 'Information flow and cooperative control of vehicle formations', *IEEE Trans. Autom. Control*, 2004, **49**, (9), pp. 1465–1476

[9] OLFATI-SABER R.: 'Flocking for multi-agent dynamic systems: algorithms and theory', *IEEE Trans. Autom. Control*, 2006, **51**, (3), pp. 401–420

[10] LEE D., SPONG M.W.: 'Stable flocking of multiple inertial agents on balanced graphs', *IEEE Trans. Autom. Control*, 2007, **52**, (8), pp. 1469–1475

[11] XIE G., WANG L.: 'Consensus control for a class of networks of dynamic agents', *Int. J. Robust Nonlinear Control*, 2007, **17**, (10–11), pp. 941–959

[12] REN W., ATKINS E.M.: 'Distributed multi-vehicle coordinated control via local information exchange', *Int. J. Robust Nonlinear Control*, 2007, **17**, (10–11), pp. 1002–1033

[13] REN W.: 'On consensus algorithms for double-integrator dynamics', *IEEE Trans. Autom. Control*, 2008, **53**, (6), pp. 1503–1509

[14] CHUNG S.-J.: 'Nonlinear control and synchronization of multiple Lagrangian systems with application to tethered formation flight spacecraft'. PhD dissertation, Massachusetts Institute of Technology, Cambridge, MA, 2007

[15] REN W., BEARD R.W., ATKINS E.M.: 'Information consensus in multivehicle cooperative control: collective group behavior through local interaction', *IEEE Control Syst. Mag.*, 2007, **27**, (2), pp. 71–82

[16] OLFATI-SABER R., FAX J.A., MURRAY R.M.: 'Consensus and cooperation in networked multi-agent systems', *Proc. IEEE*, 2007, **95**, (1), pp. 215–233

[17] PAVONE M., FRAZZOLI E.: 'Decentralized policies for geometric pattern formation and path coverage', *ASME J. Dyn. Syst. Meas. Control*, 2007, **129**, pp. 633–643

[18] REN W.: 'Collective motion from consensus with cartesian coordinate coupling – part I: single-integrator kinematics'. Proc. IEEE Conf. on Decision and Control, Cancun, Mexico, December 2008, pp. 1006–1011

[19] REN W.: 'Collective motion from consensus with cartesian coordinate coupling – part II: double-integrator kinematics'. Proc. IEEE Conf. on Decision and Control, Cancun, Mexico, December 2008, pp. 1012–1017

[20] AGAEV R., CHEBOTAREV P.: 'On the spectra of nonsymmetric Laplacian matrices', *Linear Algebr. Appl.*, 2005, **399**, pp. 157–178

[21] CAO Y., REN W.: 'Distributed consensus for fractional-order systems: dynamic interaction and absolute/relative damping'. Proc. IEEE Conf. on Decision and Control, Shanghai, China, 2009, accepted

[22] CAO Y., REN W., SORENSEN N., BALLARD L., REITER A., KENNEDY J.: 'Experiments in consensus-based distributed cooperative control of multiple mobile robots'. IEEE Int. Conf. on Mechatronics and Automation, Harbin, China, August 2007, pp. 717–722

[23] REN W., CAO Y.: 'Convergence of sampled-data consensus algorithms for double-integrator dynamics'. Proc. IEEE Conf. on Decision and Control, Cancun, Mexico, December 2008, pp. 3965–3970

[24] LAUB A.J.: 'Matrix analysis for scientists and engineers' (SIAM, Philadelphia, PA, 2005)

8 Appendix

Lemma 4 (Schur's formula): Let $A, B, C, D \in \mathbb{R}^{n\times n}$. Let $M = \begin{bmatrix} A & B \\ C & D \end{bmatrix}$. Then $\det(M) = \det(AD - BC)$, where $\det(\cdot)$ denotes the determinant of a matrix, if A, B, C and D commute pairwise.

Lemma 5 [23]: The polynomial $s^2 + as + b = 0$, where $a, b \in \mathbb{C}$, has all roots within the unit circle if and only if all roots of $(1 + a + b)t^2 + 2(1 - b)t + b - a + 1 = 0$ are in the open left half plane (LHP).

Lemma 6 [24]: Let $U \in \mathbb{R}^{p\times p}$, $V \in \mathbb{R}^{q\times q}$, $X \in \mathbb{R}^{p\times p}$ and $Y \in \mathbb{R}^{q\times q}$. Then $(U \otimes V)(X \otimes Y) = UX \otimes VY$. Let $A \in \mathbb{R}^{p\times p}$ have eigenvalues β_i with associated eigenvectors $f_i \in \mathbb{C}^p$, $i = 1, \ldots, p$, and let $B \in \mathbb{R}^{q\times q}$ have eigenvalues ρ_j with associated eigenvectors $g_j \in \mathbb{C}^q$, $j = 1, \ldots, q$. Then the pq eigenvalues of $A \otimes B$ are $\beta_i\rho_j$ with associated eigenvectors $f_i \otimes g_j$, $i = 1, \ldots, p, j = 1, \ldots, q$.

Lemma 7 [4]: Let $\mathcal{L}$ be the non-symmetric Laplacian matrix associated with the weighted directed graph $\mathcal{G}$. Then $\mathcal{L}$ has at least one zero eigenvalue and all non-zero eigenvalues have positive real parts. Furthermore, $\mathcal{L}$ has a simple zero eigenvalue and all other eigenvalues have positive real parts if and only if $\mathcal{G}$ has a directed spanning tree. In addition, there exist $\mathbf{1}_n$ satisfying $\mathcal{L}\mathbf{1}_n = 0$ and $\mathbf{p} \in \mathbb{R}^n$ satisfying $\mathbf{p} \geq 0$, $\mathbf{p}^{\mathrm{T}}\mathcal{L} = 0$, and $\mathbf{p}^{\mathrm{T}}\mathbf{1} = 1$ (That is, $\mathbf{1}_n$ and $\mathbf{p}$ are, respectively, the right and left eigenvectors of $\mathcal{L}$ associated with the zero eigenvalue.).

Lemma 8 (see [18, 19]): Given a rotation matrix $R \in \mathbb{R}^{3\times 3}$, let $\mathbf{a} = [a_1, a_2, a_3]^{\mathrm{T}}$ and θ denote, respectively,

doi: 10.1049/iet-cta.2009.0338

the Euler axis (i.e. the unit vector in the direction of rotation) and Euler angle (i.e. the rotation angle). The eigenvalues of R are 1, $e^{\iota\theta}$ and $e^{-\iota\theta}$ with the associated right eigenvectors given by, respectively, $\varsigma_1 = \mathbf{a}$, $\varsigma_2 = [(a_2^2+a_3^2)\sin^2(\theta/2),\ -a_1a_2\sin^2(\theta/2)+\iota a_3\sin(\theta/2)|\sin(\theta/2)|,\ -a_1a_3\sin^2(\theta/2)-\iota a_2\sin(\theta/2)|\sin(\theta/2)|]^{\mathrm{T}}$ and $\varsigma_3 = \overline{\varsigma_2}$, The associated left eigenvectors are, respectively, $\varpi_1 = \varsigma_1$, $\varpi_2 = \overline{\varsigma_2}$, and $\varpi_3 = \overline{\varsigma_3}$.